

See discussions, stats, and author profiles for this publication at: <https://www.researchgate.net/publication/351567745>

Quenching Mechanism of Uranyl(VI) by Chloride and Bromide in Aqueous and Non-Aqueous Solutions

Article in *The Journal of Physical Chemistry A* · May 2021

DOI: 10.1021/acs.jpca.1c02487

CITATIONS

0

READS

51

6 authors, including:



Toni Haubitz

Universität Potsdam

10 PUBLICATIONS 30 CITATIONS

[SEE PROFILE](#)



Björn Drobot

Helmholtz-Zentrum Dresden-Rossendorf

29 PUBLICATIONS 352 CITATIONS

[SEE PROFILE](#)



Satoru Tsushima

Helmholtz-Zentrum Dresden-Rossendorf

107 PUBLICATIONS 2,133 CITATIONS

[SEE PROFILE](#)



Robin Steudtner

Helmholtz-Zentrum Dresden-Rossendorf

52 PUBLICATIONS 589 CITATIONS

[SEE PROFILE](#)

Some of the authors of this publication are also working on these related projects:



Siderophores new synthetic [View project](#)



Sorption of actinides and fission product in brine [View project](#)

Quenching Mechanism of Uranyl(VI) by Chloride and Bromide in Aqueous and Non-Aqueous Solutions

Toni Haubitz, Björn Drobot, Satoru Tsushima, Robin Steudtner, Thorsten Stumpf, and Michael U. Kumke*



Cite This: <https://doi.org/10.1021/acs.jpca.1c02487>



Read Online

ACCESS |



Metrics & More

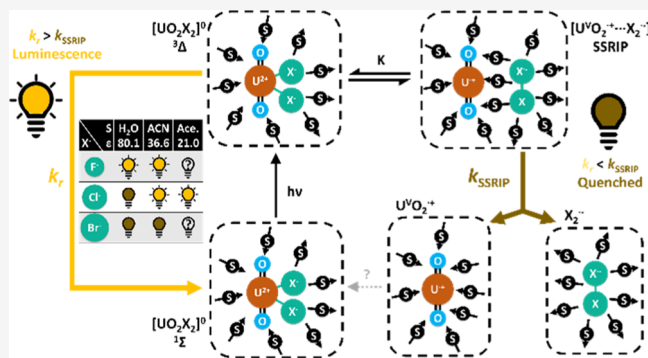


Article Recommendations



Supporting Information

ABSTRACT: A major hindrance in utilizing uranyl(VI) luminescence as a standard analytical tool, for example, in environmental monitoring or nuclear industries, is quenching by other ions such as halide ions, which are present in many relevant matrices of uranyl(VI) speciation. Here, we demonstrate through a combination of time-resolved laser-induced fluorescence spectroscopy, transient absorption spectroscopy, and quantum chemistry that coordinating solvent molecules play a crucial role in U(VI) halide luminescence quenching. We show that our previously suggested quenching mechanism based on an internal redox reaction of the 1:2-uranyl-halide-complex holds also true for bromide-induced quenching of uranyl(VI). By adopting specific organic solvents, we were able to suppress the separation of the oxidized halide ligand X_2^- and the formed uranyl(V) into fully solvated ions, thereby “reigniting” U(VI) luminescence. Time-dependent density functional theory calculations show that quenching occurs through the outer-sphere complex of U(VI) and halide in water, while the ligand-to-metal charge transfer is strongly reduced in acetonitrile.



INTRODUCTION

Health risk of humans due to exposure to uranium includes radiological as well as chemical toxicity.¹ The average U concentration in drinking water among OECD countries varies between 0.9 ng L⁻¹ and 0.4 μg L⁻¹. A small supplier may have a much higher level of U as in the case of a private supplier in Canada who reported a U concentration as high as 700 μg L⁻¹.² Uranium content in aquifers is of potential health concern and establishment of an *in situ* measuring technique is indispensable. Time-resolved laser-induced fluorescence spectroscopy (TRLFS) is one of the most promising techniques for such purposes due to its outstanding sensitivity and selectivity.³ Each U(VI) species exhibits a characteristic luminescence spectrum and a corresponding luminescence decay time, allowing spectral deconvolution to get a species distribution from mixed samples. Recently, we demonstrated that U(VI) speciation in a given U(VI) solution of micromolar concentration over a wide pH range can be obtained through a combination of TRLFS and parallel factor analysis (PARAFAC).⁴ This principle can be applied to many environmental-relevant U(VI) systems but is often hindered due to quenching by coexisting matrix compounds. Various organic and inorganic substances are known to quench U(VI) luminescence.⁵ For instance, most aqueous U(VI) complexes with carbonate and chloride are non-luminescent or only minimal luminescent at room temperature.^{6,7} Carbonate and chloride

are both environmentally abundant and quenching by these ions is consequently a critical problem for the determination of U(VI) speciation in the real-world samples. The mechanism of U(VI) luminescence quenching has been intensively studied both experimentally and theoretically.^{5,7-13} Whereas experimental studies focused primarily on *dynamic* quenching, theoretical calculations were performed exclusively on *static* quenching in [UO₂²⁺X]⁺ (X = Cl⁻, Br⁻, I⁻). This gap will be addressed in the present investigation. We found that U(VI) luminescence quenching by halide ions is getting suppressed when solvent water is replaced by acetonitrile (ACN) or acetone (Ace.). This motivated us to revise our previous model on the mechanism of chloride-induced quenching of U(VI) emission.¹³ Here, we investigate the influence of chloride and bromide in aqueous solution in a large concentration range of 0–1 and 0–0.1 M, respectively, and discuss differences found for uranyl(VI) with chloride in ACN solution.

Received: March 19, 2021

Revised: April 30, 2021

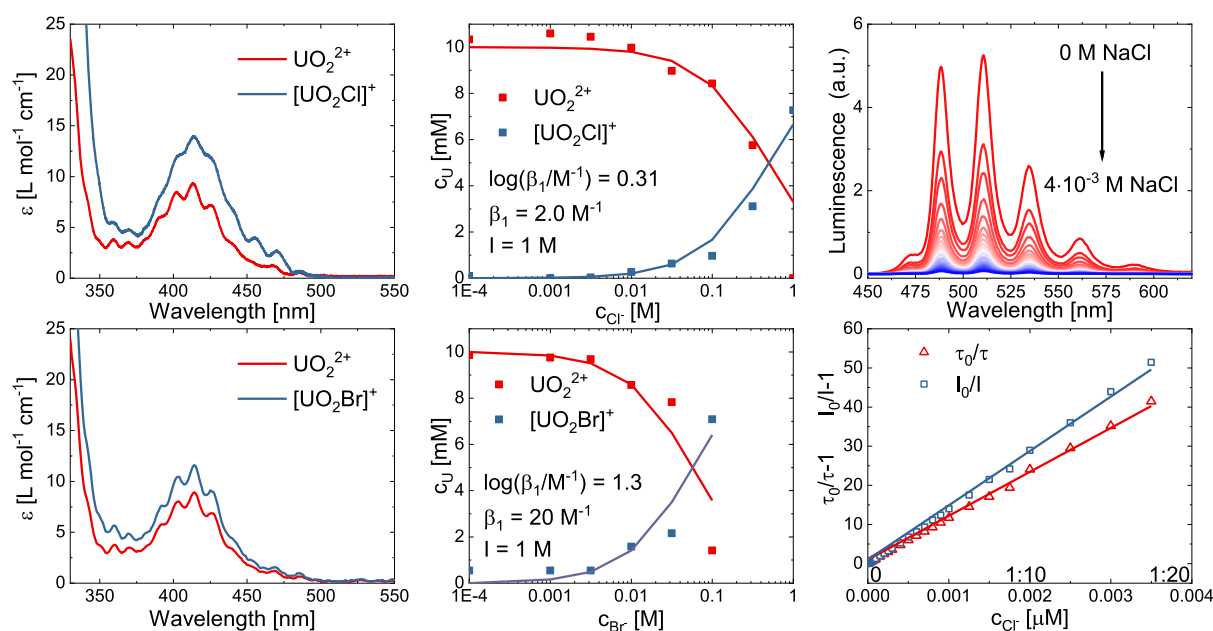


Figure 1. Spectroscopic results of the investigated samples. Left: PARAFAC deconvoluted UV/Vis data of the free uranyl(VI) and the first chloride complex (top) and the first bromide complex (bottom). Center: PARAFAC deconvoluted speciation plot with fitted complex stability constants and extinction coefficients from UV/Vis data of the free uranyl(VI) and the first chloride complex (top) and the first bromide complex (bottom). Right: U(VI) luminescence spectra with increasing NaCl concentration (top) and its Stern–Volmer plot (bottom). Experimental conditions: UV/vis: $c_U = 0.01 M$, $c_{Cl} = 0–1 M$, $c_{Br} = 0–0.1 M$, $pH \approx 0$, $I = 1 M$ (HClO₄). Luminescence: $pH 2$, U(VI) $2 \times 10^{-5} M$, $0 \leq Cl^-/UO_2^{2+} \leq 20$, and $0.1 M NaClO_4$.

EXPERIMENTAL SECTION

A uranyl(VI) stock solution was prepared by dissolving solid UO₃ in HClO₄. The final uranyl(VI) concentration in each sample for the transient absorption measurement was set to be $(0.098 \pm 0.001) M$ (checked by ICP–MS) to receive a maximum signal with a low degree of self-quenching.

The pH values were measured by a double junction pH electrode Profitrode 125 mm from Merck with a 3 M NaClO₄ solution as a bridge electrolyte, to avoid chloride contamination by the electrode. For dilution, deionized water was used and was generated by a Milli-Q Reference Water Purification System of Merck Millipore to 18.2 M Ω . All measurements were performed at room temperature ($T = 295 K$) if not stated otherwise.

As background electrolyte, 1 M perchloric acid was chosen in all samples. To adjust the ligand concentrations, for chloride samples, 1 M hydrochloric acid, while for the bromide sample, 1 M sodium bromide solutions were used as complexation agents that replaced the background electrolyte accordingly. This procedure results in samples with a pH of about 0 if not stated otherwise. However, for higher concentrated bromide samples, the pH might be slightly higher. In the highest concentrated bromide sample of 0.1 M NaBr, nine parts of the solution were 1 M perchloric acid and one part was 1 M NaBr solution. This equates to a maximum ΔpH of about 0.05. For measurements in ACN, LiBr and LiCl were used.

TRLFS measurements were conducted with a quadrupled Nd:YAG Laser (Minilite, Continuum) at 266 nm using a 0.3 mJ per 5 ns pulse. For detection, a iHR550 spectrograph and an iCCD camera (Horiba Jobin Yvon, 100 lines/mm grid) with a spectral resolution of 0.2 nm were used. UV/Vis measurements were performed on a CARY 5G spectrometer (Varian) with a spectral resolution of 0.1 or 1 nm. In both

cases, the samples were measured in 4 mL quartz cuvettes with a 1 cm pathway (Hellma Analytics).

Photoluminescence measurements were performed on a QuantaMaster 40 spectrofluorometer (PTI, now Horiba) equipped with a 75 W xenon arc lamp. Excitation and emission wavelengths were chosen by corresponding motorized monochromators with a bandwidth of 10 and 2 nm, respectively. Spectra were recorded by scanning emission with 1 nm resolution and an integration time of 1 s. Temperature constants was achieved via a temperature controllable cuvette holder (TC125 Temperature Control, Quantum Northwest).

The PARAFAC algorithm,¹⁴ implemented in the optimization toolbox of Matlab 2017 (MathWorks),¹⁵ was utilized to deconvolute the spectra and time traces into the single contained species. A numerical approach has been chosen to fit a kinetic model to the deconvoluted time traces, in which the corresponding ordinary differential equations (ODEs) of the model were solved by the ODE45 algorithm in Matlab 2017 (MathWorks). The rate constants k of the rate equations were varied to achieve a least square minimum between the numeric model and the experimental time traces by the fmincon algorithm.

Quantum chemical calculations were performed using the Gaussian 09 program employing the density functional theory (DFT) by using a conductor-like polarizable continuum model in ACN ($\epsilon = 36.64$) as previously described.⁴ Structure optimizations were performed at the B3LYP level followed by vibrational frequency analysis at the same level to confirm no imaginary frequencies are present. For the calculations of the lowest lying triplet states, two approaches were taken. First, single configuration DFT was used and spin multiplicity of molecules was set to triplet and the lowest lying state structure was achieved. Second, non-equilibrium time-dependent DFT (TD-DFT) calculations were applied to obtain lowest lying

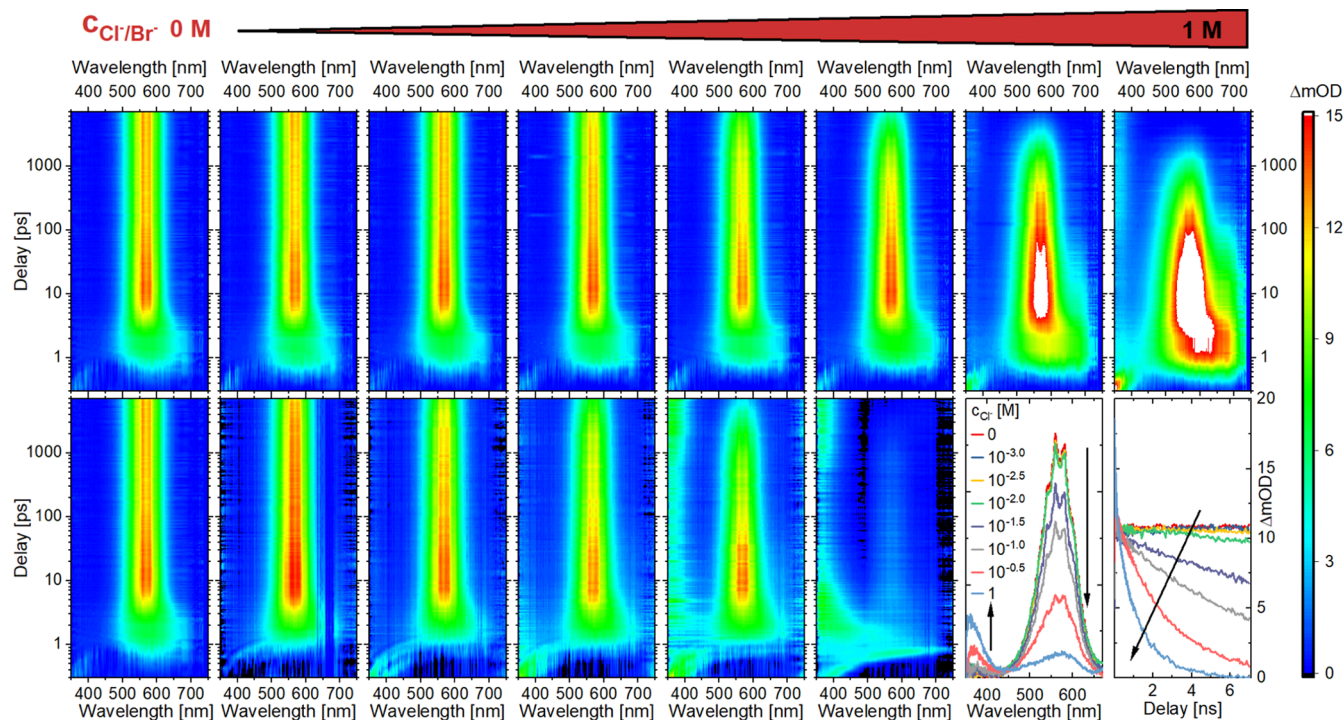


Figure 2. Transient absorption spectra of uranyl(VI) solutions at eight different chloride concentrations (top row) and six different bromide concentrations (bottom row, left). Bottom right: Transient Spectra (at 7 ns delay) and time traces (at 550 nm) of the chloride samples. $c_{\text{U}} = 0.01$ M, $c_{\text{Cl}} = 0\text{--}1$ M, $c_{\text{Br}} = 0\text{--}0.1$ M, $\text{pH} \approx 0$, $I = 1$ M, $\lambda_{\text{exc}} = 310$ nm, $E_{\text{pulse}} = 4$ μJ , $\tau_{\text{IRF}} = 100$ fs.

triplet state structures. For the calculations of emission energy from the triplet excited state to the ground state, state-specific non-equilibrium solvation calculations have been performed. The energy-consistent small-core effective core potential and the corresponding basis set suggested by Kuchle et al.¹⁶ were used for uranium. The most diffuse basis functions on uranium with the exponent 0.005 (all s, p, d, and f type functions) were omitted. For chlorine, oxygen, and hydrogen, the valence triple-zeta plus polarization basis was used. The spin-orbit effects and basis set superposition error corrections were neglected.

Transient absorption spectroscopy (TAS) measurements were conducted with a Titan-Sapphire-laser system Spitfire Ace PA (Spectra-Physics) as the light source ($\lambda = 800$ nm, pulse length of approximately 100 fs, repetition rate of 1 kHz). The fundamental laser beam is split into a pump and a probe beam. The pump beam wavelength was adjusted using a HE-TOPAS (Light Conversion) parametric amplifier. Unless stated otherwise, a pump wavelength of $\lambda_{\text{pump}} = 310$ nm (bandwidth $\Delta\lambda$ approx. 40 nm) was chosen, as uranyl(VI) complexes studied here can be excited in this range. Both beams were coupled into the transient absorption spectrometer (Newport). The probe beam is sent over a variable optical delay line, adjustable between 0 and 2.4 m delay path length, which corresponds to a maximum time delay between λ_{pump} and λ_{probe} of $\Delta t = 8$ ns with a maximum time resolution of 26.6 fs. For white light generation, the probe beam was coupled into a CaF_2 crystal to create a white light continuum of $350 \text{ nm} < \lambda_{\text{probe}} < 700$ nm. The transient signal (ΔOD) was calculated based on the logarithmic ratio between the white light intensity with and without a pump beam by the controller software (TAS software Newport, version 2.1). The pump power in the sample was adjusted by a neutral density filter and the resulting pump power was measured by a PEPS-3-9.5 sensor and a

1918-R power meter (Newport) prior to and after each measurement. 2 mm quartz cuvettes from Starna GmbH (Typ 21) were used for measurements and were rigorously stirred during the measurements (Electronic Stirrer model 300, Rank Brothers Ltd.).

RESULTS AND DISCUSSION

Uranyl(VI) with Halides in Aqueous Solution. Figure 1(left) shows the PARAFAC results of experimental UV/Vis data of the uranyl(VI) absorption in 0.01 M concentration at $\text{pH} \approx 0$ and $I = 1$ M (HClO_4). As can be seen, the PARAFAC deconvolution algorithm was able to extract two distinct species of uranyl(VI) for each of the raw data sets with chloride and bromide as a ligand. As the absorption spectra for the free and complexed uranyl(VI) species are very similar in shape, especially for the bromide sample, the main information source for the deconvolution of the two species was the increase in absorption upon addition of ligand, as the complexed species have a significantly higher extinction coefficient (at least 20% higher). The corresponding distribution for both of these species can be seen in Figure 1(Center). We can identify one of these species (present in both samples at a 0 M ligand concentration) as the free uranyl(VI) aquo ion.¹⁷ With increasing ligand concentration, the aquo ion is steadily replaced by the second uranyl(VI) species. It can easily be argued that this is the first uranyl(VI)–halide complex $[\text{UO}_2\text{X}]^+$, respectively. By fitting the PARAFAC normalized speciation data by least-square parameter optimization (fmincon, Matlab) of symbolically solved complex equilibria (symbolic toolbox, Matlab), we received fitted extinction coefficients ϵ and complex stability constants β_1 for both ligand samples. We can see that for the first complex stability constant β_1 , chloride ions form a 10 times' weaker complex than with bromide, 2.0 M^{-1}

(Soderholm/NEA-Database:¹⁸ 1.5 m^{-1} at $I = 5.3 \text{ m}^{-1}$) compared to 20 M^{-1} (Razik:¹⁹ 65 m^{-1} at $I = 0.05 \text{ M}^{-1}$), respectively.

Figure 1(right) shows the evolution of U(VI) emission in aqueous solution at pH 2 (no hydrolysis present at $\text{pH} < 3$ ²⁰) with increasing NaCl concentration ($0 \leq \text{Cl}^-/\text{UO}_2^{2+} \leq 20$). Species distribution changes from $[\text{UO}_2(\text{H}_2\text{O})_5]^{2+}$ (aquo ion) to uranyl(VI)–chloro complexes with increasing chloride concentration. The non-linearity of the Stern–Volmer intensity plot as well as the smaller slope of the lifetime plot indicate a combination of dynamic quenching (*via* $\text{UO}_2^{2+}(\text{aq})\text{–Cl}^-$ ion pair) and minor contribution of static quenching ($[\text{UO}_2\text{Cl}]^+$). In comparison to this, at pH 8 (where uranyl(VI)–chloro complexes are absent in high saline solutions²¹ and where the stronger polynuclear uranyl(VI)–hydroxo species predominate the Stern–Volmer plot, the uranyl(VI) luminescence shows different features (Figure S1). With increasing NaCl concentration, both intensity and lifetime plots show slopes close to zero, indicating complete absence of dynamic and static quenching. While prevention of static quenching is obvious because of lack of uranyl(VI)–chloro species (which are displaced by the stronger hydroxo complexes due to the higher pH), absence of dynamic quenching can be attributed to less probable ion-pair formation between negatively charged hydroxo uranyl(VI) species (stoichiometry $(\text{OH}^-)/(\text{UO}_2^{2+}) > 2$) and negatively charged chloride ions. In comparison, for the case of the positively charged UO_2^{2+} aquo ion association with Cl^- is possible as demonstrated by molecular dynamics (MD) simulations,²² thereby contributing to dynamic quenching.

In Figure 2, one can see the transient absorption spectra at $\text{pH} \approx 0$ with increasing chloride concentration. As one can see in the free uranyl(VI) spectrum (0 M chloride), the TA spectroscopy of uranyl(VI) is determined by two major features: After excitation by UV radiation a broad absorption appears, which we previously assigned as the absorption from the $^3\Phi$ into the $^3\Gamma$ state of the uranyl(VI).²³ A few picoseconds later, the signal is replaced via internal conversion by an absorption spectrum with a defined vibronic structure, which is blue-shifted in comparison to the absorption from the $^3\Phi$ state. This absorption was previously assigned to the absorption due to a transition from the $^3\Delta$ state into the $^3\Pi$ state of the uranyl(VI) and is the energetically lowest excited state from which the uranyl(VI) luminescence with several microsecond lifetime occurs. After initial population of the $^3\Delta$ state, this state remains populated within the time window accessible by the TAS setup used (observable time window of the TAS is about 7 ns). This is because with a lifetime of several microseconds, only a minimal fraction of molecules return to the ground state within the observation window. With increasing halide concentrations, we can gradually see the acceleration of the depopulation of this state, corresponding to the quenching of luminescence by halide ions. This is true for both investigated halide ions (bromide and chloride). Furthermore, it is visible that at high chloride concentrations, not only the lifetime becomes considerably shorter (below 1 ns) but also that more spectral features appear in the TA spectrum (see Figure 2). These are even broader and more red-shifted than the ones observed for the free uranyl(VI)'s $^3\Phi$ state but also have a longer lifetime and a stronger absorption than in the $^3\Delta$ state. These additional features can be assigned to (1) the complex formation of $[\text{UO}_2\text{Cl}]^+$ and (2) the formation of photoproducts.

At 1 M concentration, it is visible that at 360 nm and after 20 ps, a signal starts to evolve, which we assigned to the formation of the dichloride radical $\text{Cl}_2^{\bullet-}$. This radical forms when the excited $[\text{UO}_2\text{Cl}]^+$ complex collides with an additional chloride ion and the chloride is being oxidized by the excited uranyl(VI) (electrochemical potential of excited uranyl(VI) about +2.61 V,²⁴ comparable to elemental fluorine). This process is the origin for the uranyl(VI)'s phosphorescence typical dynamic quenching character in the presence of chlorides. The previously determined mechanism for this is that the collision forms the excited $[\text{UO}_2\text{Cl}_2]^0$ complex, which immediately undergoes a redox reaction, where a ligand to metal electron transfer occurs. After this charge transfer, the transient species $\text{U(V)O}_2^+\text{–Cl}_2^{\bullet-}$ radical complex is present, which is shortly after separating into two fully solvated separate ions of U(V)O_2^+ and $\text{Cl}_2^{\bullet-}$. This separation is then the actual quenching mechanism of the excited state. As both molecules are present in their fully separated solvated ground state, the transient absorption spectra represent their ground state absorption spectra. It is well known that U(V)O_2^+ is not stable in aqueous solution and will undergo disproportionation into uranyl(VI) and uranium (IV) within a few milliseconds under our sample conditions.²⁵ However, any forming uranium (IV) and uranyl(V) are not long-term stable under aerobic conditions and will be at some point reoxidized by $\text{Cl}_2^{\bullet-}$, its products, or solvated oxygen to uranyl(VI) due to its higher electrochemical potential, completing the cycle with the sample being practically unchanged and the luminescence quenched.

Bromide shows a very similar luminescence quenching behavior in comparison to chloride in water (Figure S2). To control the postulated mechanism to also apply to the uranyl(VI)–bromide-system and to separate the raw data into single component spectra and their respective temporal behavior, all spectra were globally analyzed and deconvoluted by a PARAFAC analysis. As dimensions for the deconvolution tensor, we used the wavelength, delay time, and excitation energy (two different energies were used for the collection of the TA spectra). As the temporal behavior changes from sample to sample for each component (which is not covered by the PARAFAC model), we combined all time traces into one “stacked” time trace. This means the time vector had a length of not only 681 datapoints (one complete TA spectrum with 681 different delay steps) but also $681 \times 8 \times 3$ (data points \times samples \times scans per sample). The full tensor has then the dimension energies \times delay \times wavelength. The fit was done under non-negative constraints on all three dimensions until good enough starting values were found to loosen the constraint on the time domain (noise around $\Delta\text{OD} = 0$ is typical for TAS). From this deconvolution, we recovered five different species for the chloride samples and three different species for the bromide samples. Next to the four found in our previous publication, we were able to separate the $^3\Delta$ state of the free and the complexes from one another. This was made possible based on the additional data points for intermediate halide concentrations.

For the bromide samples however, as the 1:0- and 1:1-complexes are spectrally very similar in luminescence,²⁶ it can be assumed that their transient spectra are also very similar and are difficult to be separated spectrally due to the broad character of transient absorptions. Additionally, their temporal behavior is coupled via the complexation equilibrium, which makes them both appear as one component in a PARAFAC

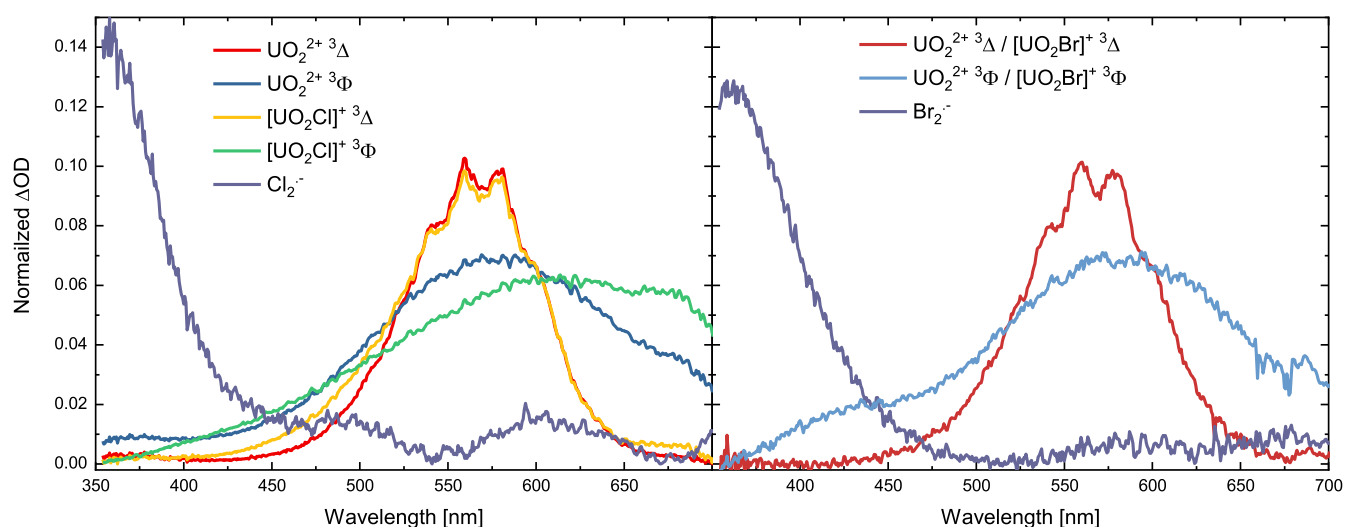


Figure 3. PARAFAC deconvoluted spectra of uranyl(VI) species in chloride (left) and bromide (right) samples. For bromide, PARAFAC was able to differentiate the different states but not the different complexes. $c_U = 0.01$ M, $c_{Cl} = 0-1$ M, $c_{Br} = 0-0.1$ M, $pH \approx 0$, $I = 1$ M.

deconvolution and leading to a reduced number of components observable in the bromide samples.

As can be seen in Figure 3, the spectra of the free uranyl(VI) and its complexes are very similar, in energy as well as in shape. However, the bromide complex signals are slightly red-shifted ((0.7 ± 0.2) nm) compared to the chloride signals. The energetic structure of the transient absorption represents the vibronic pattern of the absorption, meaning that absorptions not only are conducted into the lowest vibronic state of the electronically excited state but also into higher vibronic states as well. This means that the energetic difference in the vibronic pattern represents the vibrational energies of the molecule, for example, the symmetric or antisymmetric stretch vibration of the $^3\Pi$ state.

The dihalide radical signals fit well with the literature data, where the maximum of the dichloride radical of 340 nm²⁷ is not detectable by the transient spectrometer (lower limit 350 nm) and the maximum of the dibromide radical is found to be 361 nm (Lit. 360 nm²⁷).

Furthermore, no uranium (IV) or uranyl(V) transients were detected, which might be due to a mismatch in excitation wavelength, low extinction coefficient at the excitation wavelength of the ground state, low concentration, and/or low extinction coefficients in the observed spectral window of the excited states of these ions.

The deconvoluted time traces (Figures S3 and S4) give insights on how the involved electronic states and species are interconnected. A general mechanistic scheme based on our previous findings²³ can be seen in Figure 4: While the three electronic states of each complex ($^1\Sigma$ ground state, $^3\Phi$ and $^3\Delta$ excited states) are coupled via excitation, internal conversion, and intersystem crossing processes from electron orbital transitions, the complexes themselves are coupled via halide addition or abstraction kinetics, that is, complexation.

Not all depicted kinetic rates are relevant and/or necessary for a full description of the deconvoluted time profiles (overparameterization). For example, certain diffusion limited processes/pathways (like the equilibration of the first excited complex by k_5) are usually much slower than certain electronic processes (internal conversion, vibrational relaxation) and can therefore not compete with the faster processes. Also, depending on the halide (hard/soft character, size, properties),

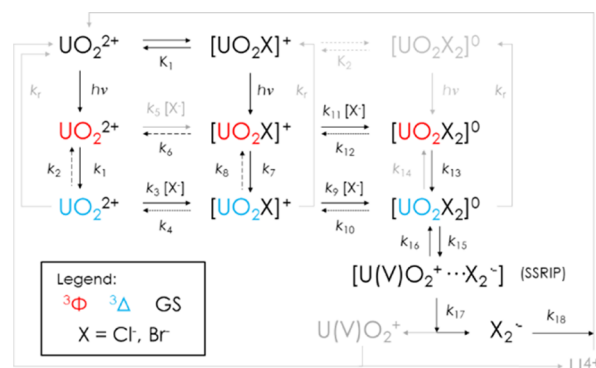


Figure 4. Kinetic scheme of possible excitation, complexation, internal conversion, and redox pathways. Lines depicted in gray: not utilized for kinetic modeling; dashed lines: kinetic pathways only relevant for chloride kinetic modeling; pointed lines: kinetic pathways only relevant for bromide kinetic modeling. $k_{17} \approx 0$ in frozen or low dielectric solvents.

certain complex formation equilibria can be or cannot be observed in the measured concentration range. Furthermore, the luminescence rates k_r will not be observed by the transient absorption spectrometer as being far too slow ($k_r < 0.01$ ns⁻¹) and thus being outside of the detection range of the instrument. These irrelevant rates were set to zero in the ODE solver and thus ignored in the numerical fitting.

The kinetic fitting of the model to the data was conducted by numerically solving the ODE of the model (see eq S1 for differential equations) and then least-square fitting of the involved rates k and relative extinction coefficients of the states (fmincon, Matlab) to the generated time profiles by the ODE solver (ODE45, Matlab). Ground state uranyl- and complex-concentrations were fully modeled in terms of the fitted complex stability constant β_1 (UV/Vis data, vide supra), as a simple one step complexation gives an analytically solvable law of mass action. Relative extinction coefficients were treated relative to uranyl(VI) ground state absorption (setting ϵ equal to 1 L mol⁻¹ cm⁻¹) for each state and species to account for different absorption intensities.

The most important rates and ground state complex stability constants can be found in Table 1. From the fitted rates, we

Table 1. Most Important Fitted Kinetic Rates k^a

	Cl ⁻	Br ⁻	unit
β_1	2	20	M ⁻¹
k_1	210	390	ns ⁻¹
k_3	45	60	ns ⁻¹ M ⁻¹
k_4	6	<0.01	ns ⁻¹
k_9	12	23	ns ⁻¹ M ⁻¹
k_{10}	<0.01	410	ns ⁻¹
k_7	1	12	ns ⁻¹
k_{13}	14	410	ns ⁻¹
k_{15}	110	580	ns ⁻¹
k_{16}	15	5.4	ns ⁻¹
k_{17}	2.2	2.9	ns ⁻¹
k_{18}	0.07	0.08	ns ⁻¹

^aGround state complex stability constants K from UV/Vis data. Complete fitted data can be found in Table S1. $c_U = 0.01$ M, $c_{Cl} = 0-1$ M, $c_{Br} = 0-0.1$ M, pH ≈ 0 , $I = 1$ M.

derive complex stability constants K_{ex} for the energetically lowest and luminescent excited states ($^3\Delta$) by taking the ratio of the formation rate and the dissociation rate ($K_{ex1} = k_3/k_4$, $K_{ex2} = k_9/k_{10}$, respectively). For the chloride ions, these are low, $K_{ex1}(Cl^-) = 7.5$ M⁻¹ and $K_{ex2}(Cl^-) > 120$ M⁻¹ ($\log_{10}(\beta_{ex1}(Cl^-)/M^{-1}) = 0.88$ and $\log_{10}(\beta_{ex2}(Cl^-)/M^{-1}) = 3.0$) and for the bromide system, $K_{ex1}(Br^-) > 6000$ M⁻¹ and $K_{ex2}(Br^-) = 0.056$ M⁻¹ ($\log_{10}(\beta_{ex1}(Br^-)/M^{-1}) > 3.7$ and $\log_{10}(\beta_{ex2}(Br^-)/M^{-1}) = 2.5$). It can be seen that both complex stability constants for both ions are, for some even several orders of magnitude, higher than for their ground state equivalents, meaning the excited state complexes are more stable (clearly visible already in raw data in Figure 2). This can be due to the elongation of one of the yl-oxygen bonds by excitation (Table 2) and thus an increased space in the equatorial plane, which leads to a closer approach of the uranium and halide ion and a better orbital overlap.

While there are large differences in complex stability constants, the photochemical and quenching behaviors for chloride and bromide are quite similar (k_{15-18}). Previously, we were not able to differentiate between the association step of the second chloride ion and the redox step.²³ We can now clearly conclude from our kinetic data that at first the second stage complex forms, which then undergoes the actual redox step to uranyl(V) and the dihalide radical $X_2^{\bullet-}$. This redox step is very rapid in comparison to the complex formation rate ($k_{15} \gg k_9$), but via a return reaction (k_{16}), a stable equilibrium between the oxidized form (radical ion pair) and the $^3\Delta$ state of the $[UO_2Cl_2]^0$ forms, which lies strongly on the side of the oxidized form ($k_{15} > k_{16}$). After this equilibrium is established, the radical ion pair complex of UO_2^+ and $X_2^{\bullet-}$ will separate into

their respective fully separated and solvated ions and no luminescent $^3\Delta$ is accessible again ($k_r \ll k_{17} = 2.2$ and 2.9 ns⁻¹, respectively). As this “separation” rate is the slowest in the whole process, it can be considered as the dominant rate competing with k_r and can be compared to the macroscopically observable quenching rate k_q in luminescence spectroscopy. Indeed, literature values for $k_q(Cl^-) = 1.9$ ns⁻¹ and $k_q(Br^-) = 4.8$ ns⁻¹ (ref 8) agree very well with the here observed rates for k_{17} .

This quenching mechanism, based on 1:2 complex formation and reduction, further explains the fact that luminescence in cryogenically frozen samples by all complexes is possible,²⁸ as the diffusion controlled dissociation step is suppressed in a frozen matrix ($k_{17} = 0$ ns⁻¹) and the equilibrium between the radical ion pair and the second stage complex (k_{15}/k_{16}) opens the possibility of a radiative deactivation pathway through the second stage complex, in other words luminescence. Furthermore, it explains the complete absence of dynamic quenching in higher pH ranges (vide supra, Figure S1), as the stronger hydroxo complexes prevent any formation of the 1:2-chloro complex.

Uranyl(VI) with Halides in Non-Aqueous Solution.

Although the quenching mechanisms discussed above do not indicate any active role of solvent molecules, it is well-known that reaction pathways including radical ion pairs are strongly affected by the solvent.²⁹ Therefore, we selected ACN as the alternative solvent for uranyl(VI) chloride luminescence studies in an attempt to manipulate excitation and deexcitation schemes. In addition to its physicochemical properties (miscible with water, certain solubility of salts), this system is useful since the U(VI)–Cl–CH₃CN system was extensively studied experimentally and theoretically.^{30–33} We measured the luminescence spectra of the U(VI)–chloride–ACN system. The well-known luminescence spectrum of uranyl(VI) aquo ion was observed in the U(VI)–ACN system in the absence of Cl⁻ as well, but with a remarkable long lifetime of ~ 30 μ s (compared to 1–4 μ s in water⁴). Addition of Cl⁻ (as LiCl) to ACN solutions did not affect the luminescence lifetime of the uranyl(VI) ion. By increasing the Cl⁻ concentration up to 0.1 M and using PARAFAC, four additional complexes were found (Figure 5, left), which correspond to a stepwise coordination of chloride to uranyl(VI). The luminescence spectrum of each species was obtained by spectral deconvolution (Figure 5, right). It was thus found that in the ACN system, the uranyl(VI)–chloro species are luminescent.

Previous works showed that as the Cl⁻ concentration increases, coordinating waters are co-substituted by chloride and ACN although the exact number of coordinating water and ACN remains somewhat ambiguous. Four chloro

Table 2. Major Bond Distances (in Å) in Singlet Ground State (S_0) and Lowest Lying Triplet State (T_1) of U(VI) Aquo, Chloro-Aquo, and Chloro-ACN Complexes and Emission Energy (in eV) from T_1 to S_0 as Obtained by DFT and TD-DFT Calculations

complex	sym.	ground state			lowest triplet			emiss.	refs.		
		U–O _{ax}	U–O _w	U–Cl	U–O _{ax}	U–O _w	U–Cl				
$[UO_2(H_2O)_5]^{2+}$	D_{5h}	1.750	2.462		1.796	2.469		2.421	23		
$[UO_2Cl(H_2O)_4]^+$	C_{2v}	¹ A ₁	1.758	2.505	2.674	³ B ₂	1.798	2.560	4.488	0.759	23
$[UO_2Cl_2(H_2O)_3]^0$	C_{2v}	¹ A ₁	1.763	2.524	2.731	³ B ₂	1.794	2.553	3.107	1.385	23
$[UO_2Cl(CH_3CN)_4]^+$	C_{2v}	¹ A ₁	1.758		2.656	³ A ₁	1.791		2.717	2.320	this work
$[UO_2Cl_2(CH_3CN)_3]^0$	C_{2v}	¹ A ₁	1.764		2.711	³ A ^o	1.797		2.745	2.360	this work

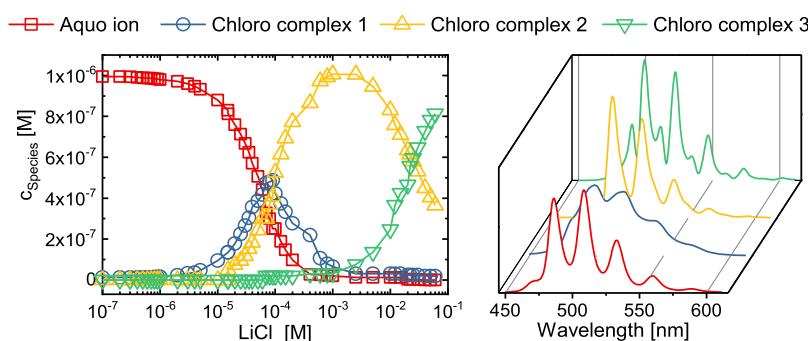


Figure 5. U(VI) species distribution with increasing LiCl concentration (left) and extracted luminescence spectra for the five independent species (right) in U(VI)–Cl–CH₃CN system. U(VI) 10^{−6} M and HClO₄ 10^{−2} M.

complexes in Figure 5 presumably correspond to the complexes with stepwise increase of chloride coordination from one to four. For DFT modeling, for the sake of simplicity, we used [UO₂Cl_{*n*}(CH₃CN)_{5−*n*}]^{2−*n*} (*n* = 1 and 2, Figure 6).

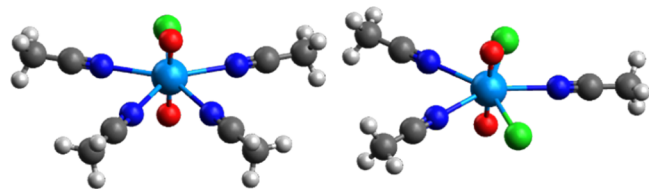


Figure 6. DFT-optimized structures of two uranyl(VI) chloro–ACN complexes [UO₂Cl(CH₃CN)₄]⁺ (left) and [UO₂Cl₂(CH₃CN)₃]⁰ (right). Uranium: light blue, oxygen: red, chlorine: green, nitrogen: dark blue, carbon: dark gray, hydrogen: white.

Deexcitation energies from T₁ to S₀ in [UO₂Cl(CH₃CN)₄]⁺ and [UO₂Cl₂(CH₃CN)₃]⁰ are 2.320 and 2.360 eV, respectively, which is close to 2.421 eV in [UO₂(H₂O)₅]²⁺ (Table 2). This corroborates the experimental results that chloride is capable of quenching U(VI) luminescence in water but not in ACN. When we examine MOs near the HOMO in U(VI)–chloride–ACN complexes, we find C 2p AOs are merged into HOMOs, whereas contribution of Cl AOs to HOMOs is clearly reduced. Thus, in U(VI)–chloride–ACN complexes, there is much reduced chloride-to-uranium charge transfer in its lowest triplet state. This indicates that other organic solvents containing carbon may have a similar trend as ACN. We tested this hypothesis using acetone and found that uranyl(VI) chloride luminescence quenching indeed does not occur in acetone (Figure S5). We thereby support our initial hypothesis that uranyl(VI) luminescence quenching is a solvent-specific phenomenon and water can be regarded as a rather peculiar solvent in this respect.

Because uranyl(VI) luminescence quenching by halides gets more pronounced as the atomic number of halide increases, quenching may be again observed in the uranyl(VI)–bromide–ACN system. We studied this point experimentally and theoretically. Figure S2 shows the Stern–Volmer plot of uranyl(VI) luminescence lifetime and intensity with increasing Br[−] concentration for the water as well as ACN system. Obviously and in contrast to Cl[−], quenching occurs for both solvents. The spin density α – β of T₁ of uranyl(VI)–bromide complexes with water and ACN coordination obtained by TD-DFT calculations are given in Figure S6, which shows bromine-to-uranyl charge transfer upon photoexcitation, thereby confirming experimental findings.

It can be seen in Figure 7 that transient spectra of uranyl(VI) with 1 M Cl[−] in ACN are similar to the water

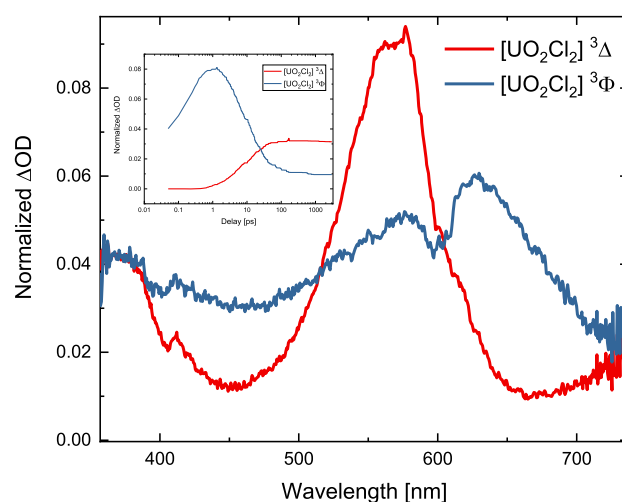


Figure 7. Deconvolution of the uranyl(VI) sample in ACN. The main graph shows the spectra, the inset shows the time profile of both excited states. Dips in spectra at 590 nm and 390 nm are laser artifacts/residuals from sum frequency generation. $c_U = 0.01$ M, $c_{Cl} = 1$ M.

samples, with the two excited states ³Φ and ³Δ and an additional absorption for a dichloride radical. However, some major differences are apparent. First, from the inset, one can see that the internal conversion between both excited states is dominated by a thermal equilibrium ($k_{13} = 650$ ns^{−1}/ $k_{14} = 97$ ns^{−1}), as the ³Φ state never reaches a ΔOD of 0 and stays present for the whole time frame accessible for the TAS setup (7 ns). By taking the ratio of the rates as an occupation ratio (in equilibrium: $N_1/N_0 = k_{14}/k_{13}$), we can calculate via a Boltzmann population at room temperature an energy gap of 407 cm^{−1} between the ³Φ and ³Δ states. Second, the lifetime of the luminescent state ³Δ is longer than the TAS observable delay time, indicating, as expected from the luminescence data, no quenching is present and an emission of luminescence despite 1 M chloride is possible. Third, the spectra of the dichloride radical and the ³Δ state could not be separated by PARAFAC. This may indicate that the radical ion pair is not separating into different species/components with their own characteristic time profiles. On the other hand, when both ions remain together in a radical ion pair, they both follow the same time profile as they remain in equilibrium and are considered by PARAFAC as one component. Furthermore, this

equilibrium supports the findings of the TD-DFT calculations, as a stable equilibrium between the oxidized and reduced forms indicates a weaker charge-transfer character in these uranyl(VI)–chloride complexes.

From these data and the established mechanism, it can be understood why the luminescence of uranyl(VI) in ACN is not quenched by chloride: the radical ion pair of uranyl(V) and the dichloride radical $\text{Cl}_2^{\bullet-}$ seem to be stable in ACN and do not break apart into separate ions with their own respective solvent shell and thus the second stage chloride complex can still luminesce similar to the solid solvent cage in frozen uranyl(VI) samples ($k_{17} = 0 \text{ ps}^{-1}$).

The reason for the different stability of radical ion pairs in different solvents is explained in literature³⁴ due to the difference in dielectric constants of the solvents (continuum approach, specific ion/solvent-interactions are ignored), where the lower dielectric constant of ACN ($\epsilon = 36.64^{35}$) makes the complexes more stable than in the high dielectric water ($\epsilon = 80.1^{35}$). The dielectric constant is a measure on how well a medium/solvent is isolating/weakening an electric field; the higher the constant, the stronger the isolation of electric fields. That means that water is very good in shielding the positive charge of the uranyl(V) radical ion from the negative charge of the dichloride radical. Thus, the Coulombic attraction between those ions reduces strongly, thus lowering the stability of the radical ion pair. The lower dielectric constant of ACN on the other hand does not isolate the charges as strongly from one another and the complex remains stable. In literature, these radical ion pairs with a shared solvent cage are usually classified as two kinds of complexes:³⁴ contact radical ion pairs (CRIPs, inner-sphere complex), where the ions stay in direct contact with one another, and solvent-separated radical ion pairs (SSRIPs, outer-sphere complex), where solvent molecules are located between both ions but they still remain a complex with one larger and shared solvation sphere. From the spectra, it is visible that both ions seem to be quantum-mechanically well separated (typical dichloride radical peak visible as if it would be fully solvated), which indicates a somewhat own solvation sphere for each ion in the complex (solvent-separated ions). Furthermore, the fact that ACN has a much lower dielectric constant but is still quite high compared to many other solvents (Gould and Farid calculated that SSRIPs dominate in ACN³⁴) and our previously found theoretical evidence for an outer-sphere complex formation²³ speak for the radical ion pair existing in a solvent-separated (SSRIP) configuration. We assume that these findings are consistent with the luminescence data in acetone (Figure S5, vide supra), where luminescence is as well present due to the formation of an SSRIP in the low dielectric medium acetone ($\epsilon = 21.01$).³⁵

In the case of bromide in ACN, the luminescence is clearly quenched again (Figure S2), so we assume that the SSRIP is not stable in the case of the bromide complexes. This might be because the dibromide radical ion is a far larger ion with the same amount of charge as the dichloride ion; thus it has a lower charge density, higher polarizability, and lower hardness. This means, in return, that the Coulombic attraction between the dibromide radical and the uranyl(V) ion is much lower than in the dichloride radical and makes the SSRIP fall apart even in the lower dielectric medium ACN and the luminescence is being quenched. This would mean that uranyl–bromide in acetone might not be quenched as the dielectric constant might be low enough to stabilize the weaker Coulombic bond between the ions.

In comparison to chloride and bromide, uranyl(VI) luminescence is not dynamically quenched by fluoride ions. This is true for the uranyl(VI)–fluoride system in water (Figure S7) as well as in ACN (Figure S8, $\tau = (1.70 \pm 0.04) \mu\text{s}$). For the 1:1 uranyl(VI)–fluoride complex, the luminescence lifetime is even strongly increased to $(52 \pm 10) \mu\text{s}$. This indicates that the higher charge density of the smaller difluoride radical ion leads to a stronger Coulombic attraction within the SSRIP, which is strong enough to stabilize the ion pair even in the highly dielectric water.

CONCLUSIONS

In this study, we investigated the validity of our previously proposed quenching mechanism of U(VI)–H₂O–chloride for a larger concentration range of chloride and for bromide as well for the non-aqueous solvent CH₃CN by TAS, luminescence spectroscopy, and theoretical calculations. Since chloride is omnipresent in majority of uranyl(VI) systems, the here presented results are of fundamental interest. Our results show that uranyl(VI) luminescence quenching by halide ions is not a general phenomenon but strongly correlated to equatorial solvent coordination.

For both halides, the dominating luminescence quenching mechanism occurs via the formation of the corresponding 1:2-complex $[\text{UO}_2\text{X}_2]^0$ and subsequent fast redox reaction to uranyl(V) and the corresponding dihalide radical $\text{X}_2^{\bullet-}$. We found that this newly formed radical ion pair remains in equilibrium with the 1:2-uranyl–halide complex. The subsequent separation into fully solvated separated ions can be described as the macroscopically observed quenching rate k_q (dynamic component), while the initial formation of the 1:1-complex $[\text{UO}_2\text{X}]^+$ is the static component of the uranyl(VI) quenching process.

By measurements in non-aqueous media, we could further show that in media with a lower dielectric constant than water, this radical ion pair does not separate into solvated independent ions but remains in close proximity as an SSRIP (outer-sphere complex). Without this dissociation step in those media, the equilibrium between the SSRIP and the 1:2-uranyl(VI)–halide-complex (re)opens a pathway for uranyl(VI)–complex luminescence and explains the less quenched behavior in non-aqueous solutions. Furthermore, this dissociation step can also not occur in aqueous media in case of a frozen sample, thus making emission possible.

Thus, we have not only explained the two quenching mechanisms but furthermore demonstrated that uranyl(VI) TAS is a useful spectroscopic technique for investigating a variety of chloride-containing uranyl(VI) systems. Furthermore, we can conclude that luminescence measurements with quenching ions in long-term repository research should be conducted under cryogenic conditions as these do not only suppress the dynamic quenching effects due to reduction but also keep the ground-state equilibrium concentration ratios fixed to guarantee measuring only the ground state and not the excited state equilibrium constants.

ASSOCIATED CONTENT

Supporting Information

The Supporting Information is available free of charge at <https://pubs.acs.org/doi/10.1021/acs.jpca.1c02487>.

Luminescence data of chloride at pH 8, quenching by bromide in ACN, fit of kinetic model to kinetic data,

emission spectra in acetone, spin densities of bromide complexes, and luminescence data with fluoride in water and ACN (PDF)

AUTHOR INFORMATION

Corresponding Author

Michael U. Kumke – Institute of Chemistry, University of Potsdam, D-14476 Potsdam, Germany; orcid.org/0000-0002-3395-9379; Email: kumke@uni-potsdam.de

Authors

Toni Haubitz – Institute of Chemistry, University of Potsdam, D-14476 Potsdam, Germany; orcid.org/0000-0003-4090-9238

Björn Drobot – Institute of Resource Ecology, Helmholtz-Zentrum Dresden-Rossendorf, D-01328 Dresden, Germany; orcid.org/0000-0003-1245-0466

Satoru Tsushima – Institute of Resource Ecology, Helmholtz-Zentrum Dresden-Rossendorf, D-01328 Dresden, Germany; Tokyo Tech World Research Hub Initiative (WRHI), Institute of Innovative Research, Tokyo Institute of Technology, 152-8550 Tokyo, Japan; orcid.org/0000-0002-4520-6147

Robin Steudtner – Institute of Resource Ecology, Helmholtz-Zentrum Dresden-Rossendorf, D-01328 Dresden, Germany; orcid.org/0000-0002-3103-9587

Thorsten Stumpf – Institute of Resource Ecology, Helmholtz-Zentrum Dresden-Rossendorf, D-01328 Dresden, Germany

Complete contact information is available at:
<https://pubs.acs.org/10.1021/acs.jpca.1c02487>

Notes

The authors declare no competing financial interest.

ACKNOWLEDGMENTS

T.H. and M.U.K. are grateful to the Federal Ministry for Economic Affairs and Energy for the financial support (contract numbers 02E11415F and 02E11860). We would like to thank H.D. Burrows for his valuable insights and preliminary measurements on the topic.

ABBREVIATIONS

TAS, transient absorption spectroscopy; PARAFAC, parallel factor analysis; TRLFS, time-resolved laser-induced fluorescence spectroscopy; IC, inner conversion; ISC, inter system crossing; LMCT, ligand to metal charge transfer; TD-DFT, time-dependent density functional theory; NIR, near infrared; ACN, acetonitrile; S, singlet; T, triplet; RIP, radical ion pair; CRIP, contact radical ion pair; SSRIP, solvent-separated radical ion pair; ODE, ordinary differential equation; MD, molecular dynamics; Ace., acetone

REFERENCES

- (1) Handley-Sidhu, S.; Keith-Roach, M. J.; Lloyd, J. R.; Vaughan, D. J. A Review of the Environmental Corrosion, Fate and Bioavailability of Munitions Grade Depleted Uranium. *Sci. Total Environ.* **2010**, *408*, 5690–5700.
- (2) WHO. *Uranium in Drinking-Water*; WHO, 2012.
- (3) Jung, E. C.; Cho, H.-R.; Cha, W.; Park, J.-H.; Baik, M. H. Uranium Determination in Groundwater Using Laser Spectroscopy. *Rev. Anal. Chem.* **2014**, *33*, 245–254.
- (4) Drobot, B.; Steudtner, R.; Raff, J.; Geipel, G.; Brendler, V.; Tsushima, S. Combining luminescence spectroscopy, parallel factor analysis and quantum chemistry to reveal metal speciation - a case study of uranyl(VI) hydrolysis. *Chem. Sci.* **2015**, *6*, 964–972.
- (5) Burrows, H. D.; Formosinho, S. J.; Miguel, M. D. G.; Coelho, F. P. Quenching of the luminescent state of the uranyl ion (UO₂²⁺) by metal ions. Evidence for an electron transfer mechanism. *J. Chem. Soc., Faraday Trans. 1* **1976**, *72*, 163–171.
- (6) Götz, C.; Geipel, G.; Bernhard, G. The Influence of the Temperature on the Carbonate Complexation of Uranium(VI): A Spectroscopic Study. *J. Radioanal. Nucl. Chem.* **2011**, *287*, 961–969.
- (7) Burrows, H. D. Electron Transfer from Halide Ions to Uranyl(2+) Excited-State Ions in Aqueous Solution: Formation and Decay of Dihalide Radical Anions. *Inorg. Chem.* **1990**, *29*, 1549–1554.
- (8) Yokoyama, Y.; Moriyasu, M.; Ikeda, S. Electron Transfer Mechanism in Quenching of Uranyl Luminescence by Halide Ions. *J. Inorg. Nucl. Chem.* **1976**, *38*, 1329–1333.
- (9) Sakuraba, S.; Matsushima, R. Photochemical Reactions of Uranyl Ions with Organic Compounds. IV. The Uranyl Fluorescence Quenching by Aliphatic Alcohols. *Bull. Chem. Soc. Jpn.* **1971**, *44*, 2915–2918.
- (10) Moriyasu, M.; Yokoyama, Y.; Ikeda, S. Quenching Mechanisms of Uranyl Luminescence by Metal Ions. *J. Inorg. Nucl. Chem.* **1977**, *39*, 2205–2209.
- (11) Yamamura, T.; Fazekas, Z.; Harada, M.; Tomiyasu, H. New Mechanism in Deactivation of Excited Uranyl(VI) Ion by Lanthanide-(III) Ions. *Phys. Chem. Chem. Phys.* **1999**, *1*, 3491–3496.
- (12) Formosinho, S. J.; Burrows, H. D.; da Graça Miguel, M.; Azenha, M. E. D. G.; Saraiva, I. M.; Ribeiro, A. C. D. N.; Khudyakov, I. V.; Gasanov, R. G.; Bolte, M.; Sarakha, M. Deactivation processes of the lowest excited state of [UO₂(H₂O)₅]²⁺ in aqueous solution. *Photochem. Photobiol. Sci.* **2003**, *2*, 569–575.
- (13) Tsushima, S.; Götz, C.; Fahmy, K. Photoluminescence of Uranium(VI): Quenching Mechanism and Role of Uranium(V). *Chem.—Eur. J.* **2010**, *16*, 8029–8033.
- (14) Bro, R. PARAFAC. Tutorial and Applications. *Chemom. Intell. Lab. Syst.* **1997**, *38*, 149–171.
- (15) MATLAB; The Mathworks Inc.: Natick, Massachusetts, 2017.
- (16) Kühle, W.; Dolg, M.; Stoll, H.; Preuss, H. Energy-adjusted pseudopotentials for the actinides. Parameter sets and test calculations for thorium and thorium monoxide. *J. Chem. Phys.* **1994**, *100*, 7535–7542.
- (17) Migdisov, A. A.; Boukhalfa, H.; Timofeev, A.; Runde, W.; Roback, R.; Williams-Jones, A. E. A spectroscopic study of uranyl speciation in chloride-bearing solutions at temperatures up to 250 °C. *Geochim. Cosmochim. Acta* **2018**, *222*, 130–145.
- (18) Soderholm, L.; Skanthakumar, S.; Wilson, R. E. Structural Correspondence between Uranyl Chloride Complexes in Solution and Their Stability Constants. *J. Phys. Chem. A* **2011**, *115*, 4959–4967.
- (19) Razik, A. A.; Ali, F. A.; Attia, F. A. Evaluation of the Stability Constants of Uranyl Association Complexes with Chloride, Fluoride, Bromide, and Sulfate Anions in Solutions of Constant Ionic Strength. *Microchem. J.* **1989**, *39*, 258–264.
- (20) Drobot, B.; Bauer, A.; Steudtner, R.; Tsushima, S.; Bok, F.; Patzschke, M.; Raff, J.; Brendler, V. Speciation Studies of Metals in Trace Concentrations: The Mononuclear Uranyl(VI) Hydroxo Complexes. *Anal. Chem.* **2016**, *88*, 3548–3555.
- (21) Hennig, C.; Tutschku, J.; Rossberg, A.; Bernhard, G.; Scheinost, A. C. Comparative EXAFS Investigation of Uranium(VI) and -(IV) Aquo Chloro Complexes in Solution Using a Newly Developed Spectroelectrochemical Cell. *Inorg. Chem.* **2005**, *44*, 6655–6661.
- (22) Nguyen, T.-N.; Duvail, M.; Villard, A.; Molina, J. J.; Guilbaud, P.; Duffrêche, J.-F. Multi-Scale Modelling of Uranyl Chloride Solutions. *J. Chem. Phys.* **2015**, *142*, 024501.
- (23) Haubitz, T.; Tsushima, S.; Steudtner, R.; Drobot, B.; Geipel, G.; Stumpf, T.; Kumke, M. U. Ultrafast Transient Absorption Spectroscopy of UO₂²⁺ and [UO₂Cl]⁺. *J. Phys. Chem. A* **2018**, *122*, 6970.
- (24) Marcantonatos, M. D. Mechanism of Interactions between Aquo-Metallic Complexes and the Photoexcited Aquo-Uranyl(VI) Ion. *J. Chem. Soc., Faraday Trans.* **1979**, *75*, 2252–2272.

- (25) Ekstrom, A. Kinetics and Mechanism of the Disproportionation of Uranium(V). *Inorg. Chem.* **1974**, *13*, 2237–2241.
- (26) Demnitz, M.; Hilpmann, S.; Lösch, H.; Bok, F.; Steudtner, R.; Patzschke, M.; Stumpf, T.; Huittinen, N. Temperature-dependent luminescence spectroscopic investigations of uranyl(vi) complexation with the halides F⁻ and Cl⁻. *Dalton Trans.* **2020**, *49*, 7109.
- (27) Hug, G. C. *Optical Spectra of Nonmetallic Transient Species in Aqueous Solutions*. National Standard Reference Data System NSRDS-NBS69, 1981.
- (28) Osman, A.; Geipel, G. *Luminescence Properties of Uranyl Ions in Chloride Media in Frozen Samples*, 2012 <https://www.hzdr.de/db/Cms?pOid=25166&pNid=1638>.
- (29) Werner, H. J.; Staerk, H.; Weller, A. Solvent, Isotope, and Magnetic Field Effects in the Geminate Recombination of Radical Ion Pairs. *J. Chem. Phys.* **1978**, *68*, 2419–2426.
- (30) Hennig, C.; Servaes, K.; Nockemann, P.; Van Hecke, K.; Van Meervelt, L.; Wouters, J.; Fluyt, L.; Görrler-Walrand, C.; Van Deun, R. Species Distribution and Coordination of Uranyl Chloro Complexes in Acetonitrile. *Inorg. Chem.* **2008**, *47*, 2987–2993.
- (31) Servaes, K.; Hennig, C.; Van Deun, R.; Görrler-Walrand, C. Structure of [UO₂Cl₄]²⁻ in Acetonitrile. *Inorg. Chem.* **2005**, *44*, 7705–7707.
- (32) Bühl, M.; Sieffert, N.; Chaumont, A.; Wipff, G. Water versus Acetonitrile Coordination to Uranyl. Density Functional Study of Cooperative Polarization Effects in Solution. *Inorg. Chem.* **2011**, *50*, 299–308.
- (33) Gaillard, C.; Chaumont, A.; Billard, I.; Hennig, C.; Ouadi, A.; Wipff, G. Uranyl Coordination in Ionic Liquids: The Competition between Ionic Liquid Anions, Uranyl Counterions, and Cl⁻ Anions Investigated by Extended X-ray Absorption Fine Structure and UV–Visible Spectroscopies and Molecular Dynamics Simulations. *Inorg. Chem.* **2007**, *46*, 4815–4826.
- (34) Gould, I. R.; Farid, S. Dynamics of Bimolecular Photoinduced Electron-Transfer Reactions. *Acc. Chem. Res.* **1996**, *29*, 522–528.
- (35) Lide, D. R. *CRC Handbook of Chemistry and Physics*, 84th ed.; CRC Press: Boca Raton, FL, USA, 2004.